Title

Non-invasive optical and laboratory hematologic biomarkers correlate in patients with sickle cell disease.

Journal

Biomedical Optics Express, 15(8)

ISSN

2156-7085

Authors

Quang, Timothy

Mostashari, Golnar

Berning, Elise

et al.

Publication Date

2024-08-01

DOI

10.1364/BOE.527770

Peer reviewed

Research Article Vol. 15, No. 8 / 1 Aug 2024 / Biomedical Optics Express 4829
Biomedical Optics EXPRESS

Non-invasive optical and laboratory hematologic biomarkers correlate in patients with sickle cell disease

TIMOTHY QUANG,[1,*] GOLNAR MOSTASHARI,[1] ELISE BERNING,[1] BINDU PARACHALIL GOPALAN,[2] MARIA A. LIZARRALDE-IRAGORRI,[2] DIANNA LOVINS,[2] ARUN S. SHET,[2] AND BRUCE J. TROMBERG[3]

[1]*National Institute of Child Health and Human Development, National Institutes of Health, Bethesda, MD 20814, USA*
[2]*National Heart, Lung, and Blood Institute, National Institutes of Health, Bethesda, MD 20814, USA*
[3]*National Institute of Biomedical Imaging and Bioengineering, National Institutes of Health, Bethesda, MD 20814, USA*
[*]*quangt2@nih.gov*

Abstract: The goal of this study is to identify non-invasive optical hemodynamic biomarkers that can index laboratory hematology measurements in sickle cell disease (SCD). We acquired frequency-domain NIRS (FD-NIRS) and diffuse correlation spectroscopy (DCS) data from the forearms and foreheads of 17 participants in a randomized, double-blind, placebo-controlled trial evaluating effects of isoquercetin (IQ) on thromboinflammation in SCD. We observed multiple, significant correlations between optical and hematology biomarkers including cerebral tissue oxygen saturation (StO_2) and hematocrit (HCT); oxyhemoglobin ($[O_2Hb]$) recovery rate and intercellular adhesion molecule 1 (ICAM-1); and blood flow index (BFI) reperfusion rate and coagulation index (CI). The potential of these non-invasive optical biomarkers for assessing vascular pathophysiology for the management of SCD warrants further exploration.

1. Introduction

Sickle cell disease (SCD) is an inherited hemoglobinopathy with widespread impact on the entire body [1,2]. Upon deoxygenation, sickled red blood cells (RBC) have altered mechanical properties and shortened lifespan [3]. These alterations disrupt microvascular flow and tissue oxygenation, which induces several processes including inflammation, endothelial dysfunction, and hypercoagulability [4,5]. Despite treatment, patients experience recurring pain crises, stroke, pulmonary hypertension, and organ failure leading to increased morbidity and mortality [1]. Clinicians can typically monitor SCD-related symptoms through laboratory assessments such as blood chemistry and medical imaging, but these approaches can be invasive or are time- and resource- intensive. In addition, patient access to more advanced clinical modalities can also be limited in low-income settings [6,7]. Due to the chronic nature of SCD, a non-invasive, continuous monitoring technology would be valuable both as a real-time assessment tool and as a predictor of SCD complications. Therefore, a clinical need exists for accurate, non-invasive, and easily accessible point-of-care technologies.

Near-infrared spectroscopy (NIRS) technologies are well-positioned to address this clinical need. They are non-invasive and uniquely sensitive to changes in microvascular hemodynamics including hemoglobin concentration, blood flow, and tissue oxygen saturation [8–11]. While NIRS clinical applications are widely reported [8,10–15], literature pertaining to NIRS in the context of SCD and its sensitivity to hemodynamic changes has been less explored. Promising work has emerged recently with regards to characterizing baseline hemodynamics of patients with SCD and monitoring hemodynamic changes due to treatment [3,16–19]. While previous analysis has mostly focused on relating optical biomarkers to laboratory hemoglobin levels, there

#527770 https://doi.org/10.1364/BOE.527770
Received 1 May 2024; revised 27 Jun 2024; accepted 4 Jul 2024; published 26 Jul 2024

Biomedical Optics EXPRESS

are a wealth of other SCD biomarkers pertaining to hemolysis, inflammation, and coagulation that optical biomarkers could index non-invasively.

Understanding which optical hemodynamic biomarkers are most reflective of SCD pathophysiology would be invaluable for developing point-of-care testing paradigms to evaluate hemodynamic status. The primary aims of this work are to 1) identify relationships between *in vivo* optical hemodynamic signatures and *in vitro* hematology biomarkers and 2) evaluate their sensitivity to changes promoted by treatment. To test these aims, we evaluated a sub-cohort of 17 SCD patients participating in a randomized, double-blind, placebo-controlled clinical trial, treated with isoquercetin (IQ, Querces Pharma AG), a plant-derived flavonoid [20]. Flavonoids have been shown to improve markers of thromboinflammation, coagulation, endothelial activation potentially reducing the occurrence of venous thromboemoblisms (VTE), and lowering mortality risk [21,22].

2. Methods

2.1. Study design

Adults with SCD who had not experienced a pain crisis 60 days prior to enrollment and were on a stable dose of hydroxyurea were recruited in a phase 2 randomized, double-blind, placebo-controlled clinical trial (ClinicalTrials.gov, #NCT04514510) [20]. This was a single institution study conducted at the National Institutes of Health (NIH) Clinical Center after ethical approval by the NIH Institutional Review Board. Participants (n = 46) were randomized to either a treatment or placebo arm with IQ to placebo allocation at a ratio of 1:1. The full trial was conducted between November 2019 to July 2022. Following a protocol amendment in December 2021, optical measurements were introduced into the study protocol. This resulted in 17 of the 46 enrolled participants having optical measurements at both the baseline visit prior to treatment initiation and the end of study (EOS) visit after 28 days of treatment with IQ or the placebo. All participants took either 1000 mg of IQ or a placebo once daily for 28 days. Cohort assignments were blinded until study completion. Table 1 summarizes the participant demographics during the baseline visit for this sub-cohort.

Table 1. Baseline demographics of the sub-cohort that underwent NIRS.[a]

Parameters	Placebo (n = 9)	Isoquercetin (n = 8)
Age (yrs)	39 ± 11	45 ± 11
Sex (M/F)	2/7	6/2
Patients on hydroxyurea	5	6
Hb (g/dL)	8.9 ± 1.9	9.3 ± 1.3
BMI	25 ± 4	26 ± 3
SATT (mm)	3.3 ± 1.5	2.2 ± 0.8
SpO_2 (%)	98 ± 2	98 ± 2

[a]SATT, Skin and adipose tissue thickness; SpO_2, peripheral tissue oxygen saturation from pulse oximetry

2.2. Instrumentation

We collected tissue hemodynamic data with a commercial, multi-modal NIRS instrument (MetaOx, ISS) [23]. This system combines two complementary NIRS modalities, frequency-domain NIRS (FD-NIRS) and diffuse correlation spectroscopy (DCS) to acquire the concentration of oxyhemoglobin ([O_2Hb]) and deoxyhemoglobin ([HHb]) as well as blood flow, respectively. The theory behind FD-NIRS and DCS has been covered extensively in other literature [10,23,24].

Biomedical Optics EXPRESS

A comprehensive description of the construction and analysis pipeline for the FD-NIRS and DCS components of the MetaOx system specifically have been described in detail by Carp et al [23]. Briefly, the FD-NIRS component sends intensity-modulated light from eight laser diodes (670 nm, 730 nm, 750 nm, 808 nm, 690 nm, 700 nm, 785 nm, 830 nm) into tissue which are detected by four photomultiplier tubes (PMTs) to measure the phase and AC amplitude of the returning signal at four source-detector separations. The frequency-domain, multi-distance method computes the tissue scattering (μ_s') and absorption (μ_a) coefficients by calculating the slope of the AC amplitude and phase vs source-detector separation (SDS) [25]. The μ_a values are then corrected for an assumed water concentration (assumed here to be 75%) [26]. Concentrations of [O_2Hb] and [HHb] are then computed via the equation, $\mu_a(\lambda) = \varepsilon_{Hb} * C$, where $\mu_a(\lambda)$ is a vector containing μ_a (corrected for water) at each wavelength, ε_{Hb} is a matrix containing the extinction coefficients for [O_2Hb] and [HHb] for each wavelength, and C is a vector containing the concentration of [O_2Hb] and [HHb]. A reference phantom ($\mu_s' = 4.8\,cm^{-1}$ $\mu_a = 0.148\,cm^{-1}$ at 760 nm, $\mu_s' = 4.2\,cm^{-1}$ $\mu_a = 0.143\,cm^{-1}$ at 830 nm) was measured prior to each measurement session for calibration.

The DCS component sends a coherent light beam into tissue and measures the intensity fluctuations caused by moving scatterers (i.e. red blood cells) which is input into an analytical model to extract a measure of flow, known as blood flow index (BFI) [10]. The DCS laser wavelength was 850 nm (Crystalaser Inc), and the output signal is detected by two 4×1 arrays of single photon counting modules. The DCS measurements are analyzed with the semi-infinite medium correlation diffusion equation [27]. Optical properties taken from simultaneous FD-NIRS measurements are incorporated into the DCS fit when calculating BFI. The scattering coefficient at 850 nm is computed by fitting linear decay curve to the $\mu_s'(\lambda)$ from the FD-NIRS wavelengths and then extrapolating μ_s' at 850 nm. The absorption coefficient is calculated by using the calculated hemoglobin concentration, assumed water concentration, and their respective extinction coefficients at 850 nm. We modeled the scatterer motion as diffusive Brownian motion, in accordance with standard practice with DCS studies [28]. An example curve fit from the DCS system averaged across all eight detectors over one second has been provided in Supplement 1 (supplementary Fig. 1). The sources and detectors for both components are all fiber-coupled and integrated into a flexible, silicone probe that can be placed at any cutaneous site. The FD-NIRS SDS' are 1.8, 2.2, 2.5, and 3.0 cm while the DCS SDS is 3.0 cm. Data from both systems are acquired simultaneously at a sampling rate of 25 Hz.

2.3. Data acquisition

Participants were seated upright for 15 minutes in the room prior to the measurement to ensure a stable, resting baseline which was then followed by a breath holding challenge and then a cuff occlusion challenge. A minimum of five minutes of rest was taken between the breath hold and cuff occlusion measurements to move the optical probe to the forearm and to explain the procedure to the patient. Figure 1 shows the system and optical probe in addition to a depiction of the probe location for both challenges with representative data from each respective site. For the breath holding challenge, the optical probe was secured to the right side of the forehead with an elastic bandage wrap. Participants were first instructed to sit at rest for one minute while breathing normally. Next, participants were instructed to exhale and hold their breath for as long as they could tolerate for up to 30 seconds; a 90 second recovery period followed each breath hold. This was repeated for three breath holds total.

For the cuff occlusion challenge, the optical probe was affixed to the right dorsal forearm and secured with an elastic bandage and the blood pressure cuff was wrapped around the right bicep; we covered the forearm with blackout cloth to minimize contributions from room lights. After collecting resting baseline measurements for three minutes, the blood pressure cuff was inflated and kept at a pressure of 200 mmHg for three minutes. A three-minute recovery period followed the occlusion. We also measured skin and adipose tissue thickness with ultrasound (Butterfly iQ,

Biomedical Optics EXPRESS

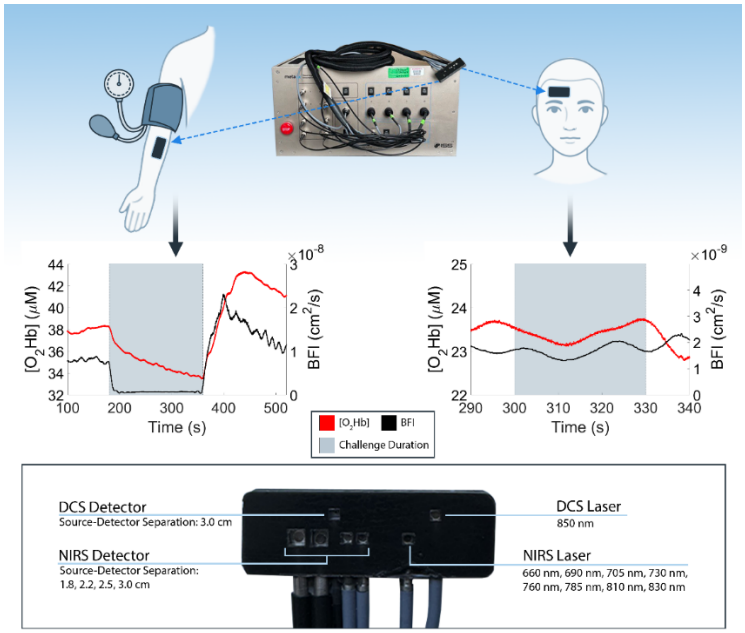

Fig. 1. Schematic diagram of the optical probe during the two challenges. A photograph of the optical probe and the multimodal optical spectroscopy device (MetaOx, ISS). Source and detector fibers for both FD-NIRS and DCS are encased in the flexible silicone pad enabling simultaneous acquisition. The probe is placed on the participant's forearm and forehead. Representative patient graphs showing [O_2Hb] and BFI for the full-length occlusion challenge (left), and during one breath hold (right). Occlusion and breath hold periods are shaded in gray.

Butterfly) at the optical probe location on the forearm. Mean SATT's for each study group is noted in Table 1.

2.4. Hematology biomarkers

Hematology and biochemical parameters were determined using anticoagulated blood from phlebotomy at least one hour prior to the NIRS measurement. A complete blood count was performed as standard of care to collect hematology parameters including hemoglobin (Hgb, g/dL) and hematocrit (HCT, %) in whole blood. In addition, thromboinflammatory markers were evaluated to evaluate the impact of IQ. In this study, whole blood samples were also analyzed with thromboelastography (TEG) within one hour of phlebotomy to determine coagulation parameters such as R-time (R), K-time (K), alpha angle (AA), and maximum amplitude (MA). From these four parameters, the coagulation index (CI) was calculated [29]. The coagulation index serves as an indicator of the global coagulation status with normal values ranging between -3 and 3. A value of -3 suggests hypocoagulability, while values exceeding 3 indicates hypercoagulability. Use of TEG markers as a clinical measure as opposed to an investigational measure varies from institution to institution. Soluble intercellular cell adhesion molecule-1 (ICAM-1), an investigational marker, was assayed in plasma with ELISA kits following the manufacturer's protocol (R&D Systems). Preparation protocols for all hematology measures can be found in Lizarralde-Iragorri et al [20].

Biomedical Optics EXPRESS

2.5. Optical biomarkers

From the FD-NIRS and DCS data, we derived metrics related to tissue composition, blood flow, tissue metabolism, and vascular reactivity. We used a type II, 4th order Chebyshev filter with 10 dB attenuation and a 0.1 Hz cutoff frequency to smooth out oscillations from the heart rate frequency for both the FD-NIRS and DCS data. Additionally, a 25-element median filter was applied to the DCS data to attenuate fluctuations associated with motion artifacts.

Resting baseline averages were calculated for both the cerebral and skeletal muscle sites. Tissue composition metrics were composed of baseline [O_2Hb] and [HHb] concentrations averaged over the baseline period. Additional derived baseline parameters were the total hemoglobin ([tHb]) concentration, defined as the sum of [O_2Hb] and [HHb], as well as tissue oxygen saturation (StO_2), defined as the ratio of [O_2Hb] to [tHb]. Mean baseline BFI was calculated in the same manner. The DCS data was additionally processed to correct for HCT given that the SCD population is known to have lower HCT. The correction used was derived from an equation previously published for cerebral blood flow using the equation: $CBF = (3*vol_{RBC}*\mu_s'_{avg}*R*BFI)/(8*\alpha_{shear}*\sigma_{RBC}*(1-g)*HCT)$ [30]. Variables in this equation are defined as follows: vol_{RBC} is the average volume of a RBC, $\mu_s'_{avg}$ is the tissue scattering measured from the FD-DCS device at 850 nm, R is the average radius of the blood vessels, α_{shear} is proportionality between shear flow rate and RBC diffusion coefficient, σ_{RBC} is RBC light scattering cross-section, and g is anisotropy factor. Assuming that the vol_{RBC}, R, α_{shear}, σ_{RBC}, and g are properties that are estimated values and will be calculated as a constant between patients, the factored BFI that accounts for the decreased HCT levels is approximated by: $BFI = \mu_s'_{avg}*BFI/HCT$.

Cerebral hemodynamics consisted of cerebral blood volume (CBV), oxygen extraction fraction (OEF), and cerebral rate of oxygen consumption ($cMRO_2$) [31]. CBV (mL/100 g) was calculated by the following expression, $([tHb]*MW_{Hb})/(Hgb * D_{bt})$; [tHb] (μM) is the total hemoglobin concentration derived from FD-NIRS, MW_{Hb} (64,500 g/mol) is the molecular weight of hemoglobin, Hgb (g/dL) is blood Hb concentration obtained from phlebotomy, and D_{bt} (1.05 g/dL) is the brain tissue density [32]. OEF (%) is defined as $(SaO_2 - StO_2)/(\beta* SaO_2)$; SaO_2 is arterial oxygen saturation which is approximated by pulse oximetry, StO_2 is the cerebral tissue oxygen saturation derived from FD-NIRS, and β (0.7) is an estimation of the contribution of the venous compartment to the microvasculature [33]. $cMRO_2$ ($cm^2/s*mL\ O_2/dL$) is defined as $1.39*Hgb*BFI*(1/\beta)*(SaO_2 - StO_2)$ [31].

Skeletal muscle hemodynamics were derived from both occlusion and post-occlusion data. We defined the rate of [HHb] change during the occlusion period as the skeletal muscle rate of oxygen consumption ($tMRO_2$) since there is no blood flow in the forearm compartment during the occlusion [34,35]. Post-occlusion hyperemic response was calculated from the [O_2Hb] and BFI traces specifically as measures of vascular reactivity [36,37]. Figure 2 shows example FD-NIRS and DCS data, the following parameters were calculated to characterize the hyperemic response from the [O_2Hb] and BFI traces: 1) reperfusion slope during the first 20 seconds after the end of occlusion, 2) recovery slope for the first 60 seconds following the hyperemic peak ($d[O_2Hb]/dt$ and dBFI/dt), 3) time elapsed from end of occlusion to hyperemic peak ($d[O_2Hb]/dt$ and dBFI/dt), 4) magnitude difference between the end of occlusion to peak of the hyperemic response, and 5) area under the curve (AUC) until the magnitude of the peak.

All data analysis was performed with a custom script developed in MATLAB 2022a (Mathworks, MA). Spearman's correlation coefficients (ρ_s) were calculated for all comparisons between optical hyperemic metrics and clinical biomarkers of endothelial function and coagulation. We also evaluated changes in optical and hematology biomarkers in both the placebo and IQ groups after treatment. Wilcoxon rank sum tests were performed to compare mean values between the different groups.

Biomedical Optics EXPRESS

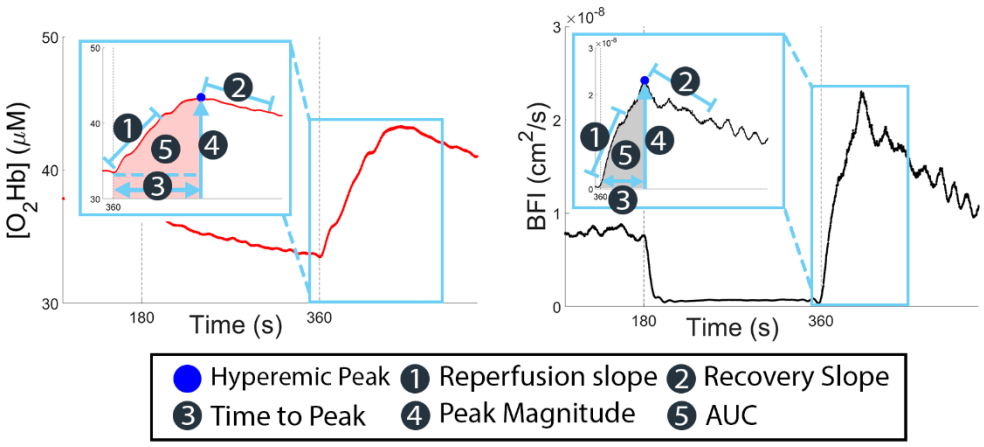

Fig. 2. Example trace of [O_2Hb] and BFI optical hemodynamic data acquired from FD-NIRS (left) and DCS (right), as well as reference points for post-occlusion metrics. Dashed lines represent the beginning and end of the occlusion period.

3. Results

We present here select correlations that had statistical significance and had a clear physiologic link between two metrics; the Spearman's rho for the remaining correlations can be found in Dataset 1 (Ref. [38]). Analysis was performed for three experimental paradigms: 1) baseline hemodynamics 2) breath-hold hemodynamics and 3) occlusion hemodynamics. During analysis, we found that breath hold responses were not consistent amongst the study group therefore we present results from the baseline and occlusion paradigms only. Measurements performed at the baseline in patients from both study arms (n = 17; IQ = 8, placebo = 9) were pooled as neither group had started the study treatment and group assignment was randomized.

3.1. Data quality control

All 17 participants in this sub-cohort were seen at baseline and 28 days later at the end of treatment, for a total of 34 visits. After data collection and analysis, participant assignments were revealed; eight patients were in the IQ group and nine patients were in the placebo group. Data were excluded for a given visit for the following reasons: 1) missing optical data, 2) poor quality optical data in which the coefficient of variation for [O_2Hb] or [HHb] exceeded 10% during baseline or if the dynamics during the occlusion perturbation could not be quantified, 3) missing hematology data, 4) patients were on any kind of additional treatment that would confound a given lab result (i.e. direct oral anticoagulants), 5) SATT was > 7 mm. The 7 mm cutoff was chosen to ensure at least 50% of the interrogated forearm volume was of skeletal muscle. Exclusion criteria were applied for each correlation performed and discussed in each upcoming section.

3.2. Baseline hemodynamics

Figure 3(A) shows the correlation between cerebral StO_2 and HCT (n = 16) and Fig. 3(B) shows the correlation between muscle StO_2 and HCT (n = 17), both during baseline visits. One baseline visit was excluded due to poor quality FD-NIRS data. We observed positive correlations between HCT and cerebral StO_2 ($\rho_s = 0.55$, $p = 0.031$). as well as HCT and muscle StO_2 ($\rho_s = 0.34$, $p = 0.18$). There was also a negative correlation between OEF and HCT at baseline ($\rho_s = -0.53$, $p = 0.036$). We did not observe any significant correlations with HCT between other baseline optical biomarkers including [O_2Hb], [HHb], [tHb], or BFI.

Biomedical Optics EXPRESS

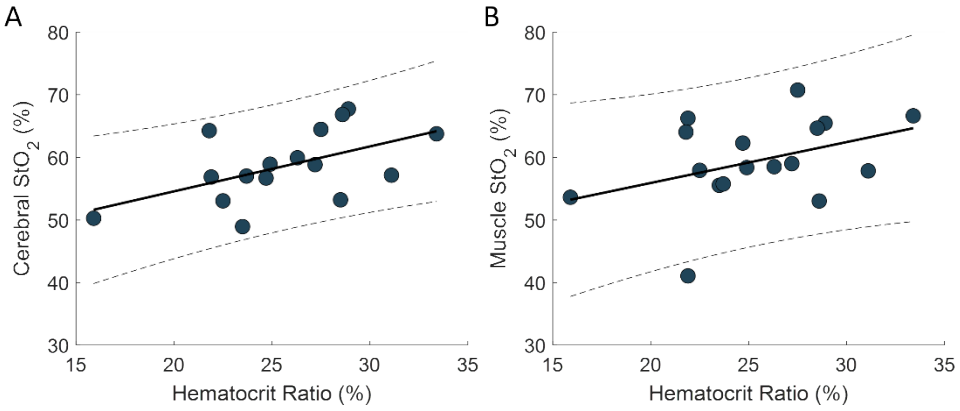

Fig. 3. A) Scatter plot of HCT and cerebral StO_2 during baseline (n = 16) and B) Scatter plot of HCT and muscle StO_2 during baseline (n = 17). Spearman's correlation coefficient was 0.55 (p = 0.031) for cerebral StO_2 and 0.34 (p = 0.18) for muscle StO_2.

Agreement between the change in both HCT and cerebral StO_2 across time in the placebo group patients was also assessed; six patients of the nine had data available for both visits. We observed 5/6 patients showed a change in cerebral StO_2 from baseline to EOS that trended in agreement with the change in HCT. Three of six patients showed increases in both cerebral StO_2 and HCT while two of the six showed no significant change in either parameter.

3.3. Occlusion hemodynamics

We next assessed correlations between skeletal muscle hemodynamic markers and hematology markers. Figure 4 shows hematology marker correlations found with both FD-NIRS data and with DCS data during the cuff occlusion challenge. The gray highlighted section in each scatter plot represents the healthy range of values for each hematology marker.

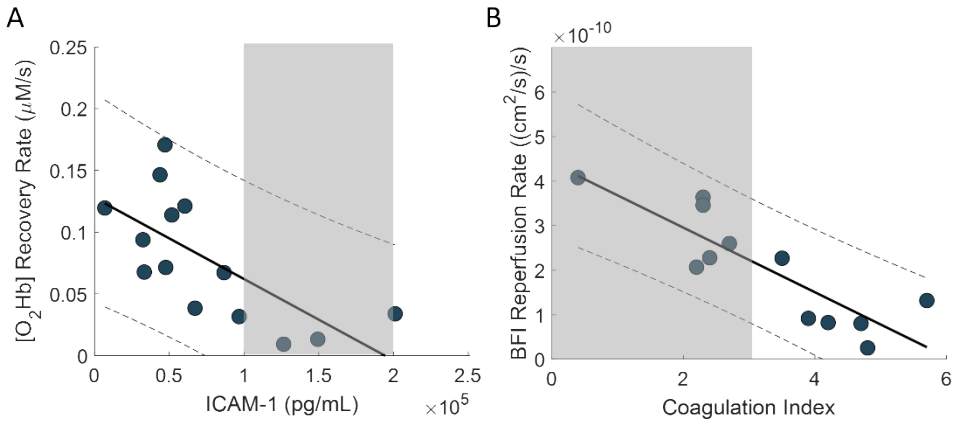

Fig. 4. Correlations between skeletal muscle hemodynamics and hematology biomarkers. Gray areas represent the healthy range of values for each hematology marker. A) Spearman's correlation coefficient between $[O_2Hb]$ recovery rate and ICAM-1 was -0.75 (p = 0.003) at baseline. B) Spearman's correlation coefficient between BFI reperfusion rate vs CI was -0.82 for baseline (p = 0.001).

Biomedical Optics EXPRESS

Figure 4(A) compares the post-hyperemic recovery rate of [O_2Hb] (d[O_2Hb]/dt), as defined in Fig. 2, with ICAM-1 for the baseline (n = 14). We found a negative correlation between ICAM and [O_2Hb] recovery slope (ρ_s = -0.75, p = 0.003). Three baseline visits were excluded due to poor FD-NIRS data quality. Seven patients in the placebo group had data available from both visits to assess agreement in the changes in ICAM-1 and [O_2Hb] recovery rate over time. We found that 4/7 patients showed a decrease in [O_2Hb] recovery rate corresponding with an increase in ICAM-1 levels across time.

Figure 4(B) compares the post-occlusion recovery slope of BFI (dBFI/dt) to the coagulation index (CI) during baseline (n = 12). Three baseline visits and one EOS visit were excluded due to poor DCS data quality; one IQ and one placebo patient were also excluded from this analysis because they were on direct oral anticoagulants which would confound the TEG readings. We found that BFI reperfusion rate, as defined in Fig. 2, negatively correlated with CI during both baseline (ρ_s = -0.82, p = 0.001) Five patients had data available at both visits to assess agreement in the change in CI and BFI reperfusion rate over time. We found that 4/5 patients showed a decrease in BFI reperfusion rate that corresponded with an increase in CI.

3.4. Impact of isoquercetin treatment

Both the study groups reported > 90% adherence to the study drug. Table 2 summarizes the changes in the hematology and optical markers after IQ treatment. The clinical outcomes of this study have been previously reported for the full cohort (n = 46) [20]. For the three hematology markers (HCT, ICAM-1, CI) that correlated with optical hemodynamic markers, we performed a Wilcoxon's signed rank test to determine if there were any statistically significant changes that occurred between the baseline and EOS visits in either the placebo or IQ groups. Statistical comparisons were performed only for patients with data available from both visits for a given parameter. We found that none of the three hematology markers showed any significant change from the baseline to the EOS visit in either group. Similarly, we found no optical marker that exhibited a significant change from baseline in either group. We compared the hematology results found in this smaller sub-cohort (n = 17) to the changes found in the full study cohort (n = 46) and found that the trends were similar between both cohorts. A full table of the mean values of all the measured optical biomarkers are included in Dataset 1 (Ref. [38]).

Table 2. Summary of changes in optical and hematology markers due to IQ treatment. Group sizes after data QC are included with each entry.

Parameters		Placebo (n = 9)		Isoquercetin (n = 8)	
	Baseline	EOS	Baseline	EOS	
Clinical	HCT (%)	25 ± 5.0	25 ± 5.0	26 ± 3.2	27 ± 3.0
	ICAM-1 (pg/mL)	90000 ± 34000 (n = 8)	107000 ± 54000 (n = 8)	58000 ± 59000	42000 ± 18000
	CI (au)	3.5 ± 1.4 (n = 8)	4.0 ± 1.1 (n = 8)	2.8 ± 1.3	1.8 ± 1.6
Optical (Cerebral)	StO_2 (%)	59 ± 6.6 (n = 6)	61 ± 9.0 (n = 6)	60 ± 4.0 (n = 5)	57 ± 3.7 (n = 5)
Optical (Muscle)	[O_2Hb] Recovery Rate (μM/s)	-0.048 ± 0.037 (n = 8)	-0.032 ± 0.024 (n = 8)	-0.10 ± 0.049	-0.10 ± 0.062 (n = 6)
	BFI Reperfusion Rate (x $10^{-10}cm^2/s^2$)	1.8 ± 1.1 (n = 6)	1.5 ± 1.5 (n = 6)	2.7 ± 1.5 (n = 6)	2.4 ± 2.4 (n = 6)

Biomedical Optics EXPRESS

4. Discussion

Non-invasive NIRS technologies are sensitive to changes in microvascular composition and function and could be a useful modality for accessible, point-of-care monitoring for patients with SCD. Identifying clinical measures that can be indexed with non-invasive optical biomarkers would facilitate data interpretation in the clinical setting by relating the changes observed in the optical markers to changes in SCD pathophysiology reflected by hematological parameters. Furthermore, there is limited work investigating the relationship between optical parameters and hematology measures in the range of values commonly seen in SCD patients. We assessed vascular hemodynamics through breath holding and cuff occlusion challenges to induce transient hemodynamic changes to reveal dynamic, physiological responses to the given perturbation. The breath holding and brachial cuff occlusion challenges have been cited previously as a non-invasive assessment of cerebrovascular reactivity and endothelial function respectively [3,15,39–41]. We did not observe a consistent breath hold response during this study potentially due to lack of patient compliance with the end-exhalation breath hold. In future work, we will improve standardization of the breath hold procedure and consider other testing paradigms such as CO_2 inhalation [42,43].

4.1. Baseline hemodynamics

With regards to cerebral hemodynamic markers, we observed that lower HCT was significantly associated with lower cerebral StO_2 values at the baseline visits ($n = 12$) as seen in Fig. 3 ($\rho_s = 0.55$, $p = 0.031$). A similar, significant negative correlation was observed between OEF and HCT ($\rho_s = -0.61$, $p = 0.012$). Although similar trends were observed for StO_2 and OEF in the EOS visits, these were not statistically significant. Lower HCT appears to be associated with lower cerebral StO_2 and increased OEF which could be related to a combination of factors including the limited oxygen carrying capacity of sickled RBC's or impaired blood flow due to vasculopathy [44]. Nahavandi et al reported that there was no significant difference in the absorption spectra of healthy and sickled hemoglobin which also seems to suggest the reduced StO_2 is due to limited oxygen carrying capacity and not to a change in the hemoglobin absorption spectra [45]. Prior work also compared StO_2, $cMRO_2$, CBV, and OEF to HCT which is consistent with the trends found in this study [46,47]. Compared to skeletal muscle StO_2, cerebral StO_2 displayed a stronger correlation to HCT potentially due to higher cerebral metabolic demand which would necessitate a change in extraction to compensate for change in oxygen availability due to lower HCT. Additionally, there could be more variability in muscle StO_2 over time related to physical activity. Individual hemoglobin species such as [O_2Hb] and [HHb] measured with FD-NIRS did not show as strong of a correlation with HCT. This is likely because HCT values represent hemoglobin concentration in blood while optically derived [O_2Hb] and [HHb] concentrations are per unit volume of tissue which would also be influenced by the blood volume fraction and how perfused the tissue is.

4.2. Occlusion hemodynamics

We also found potential correlations between hematologic markers and skeletal muscle hemodynamic markers, specifically regarding the post-occlusion hyperemic response. Increased expression of ICAM-1, an endothelial marker, showed significant correlation with a reduced [O_2Hb] recovery rate as seen in Fig. 4(A) ($\rho_s = -0.75$, $p = 0.003$). In patients with SCD, elevated ICAM-1 levels are due to the chronic ischemia-reperfusion injury promoted by continuous cycles of RBC sickling and are associated with increased cardiovascular risk and endothelial dysfunction [48,49]. The brachial cuff occlusion challenge has been reported as a test for endothelial function which lends credence to an association between ICAM-1 and FD-NIRS post-occlusion response metrics [15,41,50–52]. Increased coagulation index (CI) also showed significant correlation with

Biomedical Optics EXPRESS

reduced reperfusion rate at baseline in the BFI data (dBFI/dt) ($n = 12$, $\rho_s = -0.86$, $p = 3 \times 10^{-4}$). While we saw similar correlations in the EOS visits ([O_2Hb] recovery rate: $\rho_s = -0.46$, BFI reperfusion rate: $\rho_s = -0.67$) neither of these correlations were significant. When pooled with the EOS-IQ groups, there was a significant correlation ($n = 12$, $\rho_s = -0.74$, $p = 0.006$). TEG is an *in vitro*, point-of-care technology that can assess blood coagulation [53]. DCS is sensitive to changes in microvascular flow, which is affected by hypercoagulable blood, possibly explaining a relationship between TEG markers and DCS metrics. Previous work has reported an association between increased coagulation marker activation with endothelial dysfunction markers [54,55].

4.3. Hemodynamic changes over time

From this sub-cohort, we observed no significant change from baseline in hematology or optical markers which could be attributed to treatment with IQ. Although the sample size was small, analysis of the full cohort ($n = 46$) similarly revealed no significant changes in clinical measures [20]. Further study will be needed to test if a higher dose of IQ or a longer treatment period could promote a stronger response in the clinical measures. Due to the uncertainty of the impact of IQ on optical biomarkers, we assessed the agreement between changes over time for clinical markers and changes over time for optical biomarkers in the placebo group. We also found some agreement in the change over time between HCT vs cerebral StO_2 (5/6 agreement), ICAM-1 vs [O_2Hb] recovery rate (4/7 agreement), and CI vs BFI reperfusion rate (4/5 agreement). These longitudinal changes lend additional credence to these correlations and to the sensitivity of optical biomarkers to changes in clinical measures.

4.4. Limitations

While the trends observed in this study were promising, they would benefit from further study with a larger patient cohort to gain higher statistical confidence. DCS data from four visits had to be excluded due to low signal-to-noise from the 3 cm SDS. Optimization of the SDS for both the cerebral and muscle measurements will also be considered for future studies to maximize signal-to-noise for each anatomic site. The brain supplied more robust results compared to skeletal muscle data with regards to baseline hemodynamic parameters. Cerebral hemodynamic estimation could be improved by incorporating multilayer modeling to stratify contributions from the overlying extracerebral layer. Comparison of these results to a healthy volunteer cohort would provide better context; we are currently nearing completion of a study comparing an adult SCD cohort to a healthy volunteer cohort. We incorporated a correction factor for BFI from Benson et al to account for the low HCT observed in the SCD population [30]. While we did not incorporate all the assumed constants in the correction factor, the correlations found between BFI parameters and hematology measures should be maintained. The entire correction factor will be incorporated in future studies when comparing to a healthy population. This study was conducted with a combination of FD-NIRS and DCS which are relatively expensive and technologically complex. However, the correlations we reported could potentially be observed with more inexpensive, accessible optical techniques to measure oxygen saturation and blood flow such as continuous-wave NIRS and laser speckle imaging [17,56,57]. Although this was a small sub-analysis, the initial data highlights the potential of NIRS techniques as a non-invasive monitoring adjunct in the sickle-cell population.

5. Conclusion

We have explored correlations between non-invasive optical hemodynamic biomarkers and clinical, hematologic measures to provide further physiological context to the metrics calculated via optical techniques. Identification of non-invasive optical biomarkers that index components of SCD physiology could facilitate continuous, point-of-care options for treatment monitoring and risk stratification for SCD patients. We observed relationships between lower O_2 availability

Biomedical Optics EXPRESS

(decreased HCT) and increased extraction increased OEF, decreased cerebral StO_2. Additionally, increased expression of ICAM-1 and CI indicate greater endothelial dysfunction which can be observed through decreased post-occlusion metrics such as [O_2Hb] recovery rate and BFI reperfusion rate. Additionally, we found that changes observed in clinical measures over time were often mirrored by changes in optical biomarkers. Further study will be necessary to validate NIRS techniques as a point-of-care surrogate for hemodynamic assessment.

Funding. Eunice Kennedy Shriver National Institute of Child Health and Human Development (HD009000-01); National Heart, Lung, and Blood Institute (HL006241, HL006256).

Acknowledgments. The authors would like to thank Mai Hill and Brenda Merriweather for their work recruiting and coordinating patient study visits.

Disclosures. The authors declare no competing interests.

Data availability. Data underlying the results presented in this paper are available Dataset 1, Ref. [38].

Supplemental document. See Supplement 1 for supporting content.

References

1. M. T. Gladwin and V. Sachdev, "Cardiovascular abnormalities in sickle cell disease," J. Am. Coll. Cardiol. **59**(13), 1123–1133 (2012).
2. G. J. Kato, R. P. Hebbel, M. H. Steinberg, *et al.*, "Vasculopathy in sickle cell disease: Biology, pathophysiology, genetics, translational medicine, and new research directions," Am. J. Hematol. **84**(9), 618–625 (2009).
3. J. A. Detterich, R. Kato, A. Bush, *et al.*, "Sickle cell microvascular paradox-oxygen supply-demand mismatch," Am. J. Hematol. **94**(6), 678–688 (2019).
4. E. Saah, P. Fadaei, U. A. Gurkan, *et al.*, "Sickle Cell Disease Pathophysiology and Related Molecular and Biophysical Biomarkers," Hematol./Oncol. Clin. North Am. **36**(6), 1077–1095 (2022).
5. D. C. Rees and J. S. Gibson, "Biomarkers in sickle cell disease," Br. J. Haematol. **156**(4), 433 (2012).
6. K. I. Ataga and E. P. Orringer, "Hypercoagulability in sickle cell disease: a curious paradox," Am. J. Med. **115**(9), 721 (2003).
7. L. Lee, K. Smith-Whitley, S. Banks, *et al.*, "Reducing Health Care Disparities in Sickle Cell Disease: A Review," Public Health Rep. **134**(6), 599–607 (2019).
8. B. J. Tromberg, Z. Zhang, Anaïs Leproux, *et al.*, "Predicting responses to neoadjuvant chemotherapy in breast cancer: ACRIN 6691 Trial of Diffuse Optical Spectroscopic Imaging," Cancer Res. **76**(20), 5933–5944 (2016).
9. G. Ganesan, R V Warren, A Leproux, *et al.*, "Diffuse optical spectroscopic imaging of subcutaneous adipose tissue metabolic changes during weight loss," Int. J. Obes. **40**(8), 1292 (2016).
10. T. Durduran and A. G. Yodh, "Diffuse correlation spectroscopy for non-invasive, micro-vascular cerebral blood flow measurement," NeuroImage **85**, 51–63 (2014).
11. P. Y. Lin, N. Roche-Labarbe, M. Dehaes, *et al.*, "Non-invasive optical measurement of cerebral metabolism and hemodynamics in infants," J. Vis. Exp. **73**, e4379 (2013).
12. G. Ganesan, S. Y. Leu, A. Cerussi, *et al.*, "Cerebral and muscle tissue oxygenation during incremental cycling in male adolescents measured by time-resolved near-infrared spectroscopy," Pediatr. Exerc. Sci. **28**(2), 275 (2016).
13. N. S. Ghanayem and G. M. Hoffman, "Near infrared spectroscopy as a hemodynamic monitor in critical illness," Pediatric Critical Care Medicine **17**(8), S201 (2016).
14. H. Ayaz, W. B. Baker, G. Blaney, *et al.*, "Optical imaging and spectroscopy for the study of the human brain: status report," Neurophotonics **9**(S2), 1 (2022).
15. D. O. Cortés, L. Rahmania, M. Irazabal, *et al.*, "Microvascular reactivity is altered early in patients with acute respiratory distress syndrome," Resp. Res. **17**(1), 59 (2016).
16. M. Nahavandi, F. Tavakkoli, S. P. Hasan, *et al.*, "Cerebral oximetry in patients with sickle cell disease," Eur. J. Clin. Invest. **34**(2), 143 (2004).
17. C. M. Barriteau, F. Tavakkoli, S. P. Hasan, *et al.*, "Cerebral and skeletal muscle tissue oxygenation during exercise challenge in children and young adults with sickle cell anaemia," Br. J. Haematol. **196**(1), 179–182 (2022).
18. S. Y. Lee, A. Chiu, M. Rodeghier, *et al.*, "Noninvasive optical assessment of resting-state cerebral blood flow in children with sickle cell disease," Neurophotonics **6**(03), 035006 (2019).
19. R. O. Brothers, K. B. Turrentine, M. Akbar, *et al.*, "The influence of voxelotor on cerebral blood flow and oxygen extraction in pediatric sickle cell disease," Blood **143**(21), 2145 (2024).
20. M. A. Lizarralde-Iragorri, B. Parachalil Gopalan, B. Merriweather, *et al.*, "Isoquercetin for thromboinflammation in sickle cell disease: a randomized double-blind placebo-controlled trial," Blood Adv. **8**(1), 172–182 (2024).
21. N. P. Bondonno, F. Dalgaard, C. Kyrø, *et al.*, "Flavonoid intake is associated with lower mortality in the Danish Diet Cancer and Health Cohort," Nat. Commun. **10**(1), 3651 (2019).
22. J. I. Zwicker, B. L. Schlechter, J. D. Stopa, *et al.*, "Targeting protein disulfide isomerase with the flavonoid isoquercetin to improve hypercoagulability in advanced cancer," JCI Insight **4**(4), 1 (2019).

Biomedical Optics EXPRESS

23. S. A. Carp, P. Farzam, N. Redes, *et al.*, "Combined multi-distance frequency domain and diffuse correlation spectroscopy system with simultaneous data acquisition and real-time analysis," Biomed. Opt. Express **8**(9), 3993–4006 (2017).
24. T. D. O'Sullivan, A. E. Cerussi, D. J. Cuccia, *et al.*, "Diffuse optical imaging using spatially and temporally modulated light," J. Biomed. Opt. **17**(7), 071311 (2012).
25. S. Fantini, M. A. Franceschini, and E. Gratton, "Semi-infinite-geometry boundary-problem for light migration in highly scattering media - a frequency-domain study in the diffusion-approximation," J. Opt. Soc. Am. B **11**(10), 2128–2138 (1994).
26. A. Demel, M. Wolf, C. F. Poets, *et al.*, "Effect of different assumptions for brain water content on absolute measures of cerebral oxygenation determined by frequency-domain near-infrared spectroscopy in preterm infants: an observational study," BMC Pediatr. **14**(1), 206 (2014).
27. C. Cheung, J. P. Culver, K. Takahashi, *et al.*, "Cerebrovascular measurement combining diffuse near-infrared absorption and correlation spectroscopies," Phys. Med. Biol. **46**(8), 2053–2065 (2001).
28. K. Verdecchia, M. Diop, L. B. Morrison, *et al.*, "Assessment of the best flow model to characterize diffuse correlation spectroscopy data acquired directly on the brain," Biomed. Opt. Express **6**(11), 4288 (2015).
29. D. Whiting and J. A. DiNardo, "TEG and ROTEM: technology and clinical applications," Am. J. Hematol. **89**(2), 228 (2014).
30. E. J. Benson, D. I. Aronowitz, R. M. Forti, *et al.*, "Diffuse optical monitoring of cerebral hemodynamics and oxygen metabolism during and after cardiopulmonary bypass: hematocrit correction and neurological vulnerability," Metabolites **13**(11), 1153 (2023).
31. S. Fantini and A. Sassaroli, "Frequency-domain techniques for cerebral and functional near-infrared spectroscopy," Front. Neurosci. **14**, 300 (2020).
32. H. H. Cheng, S. L. Ferradal, R. Vyas, *et al.*, "Abnormalities in cerebral hemodynamics and changes with surgical intervention in neonates with congenital heart disease," J. Thorac. Cardiovasc. Surg. **159**(5), 2012–2021 (2020).
33. H. M. Watzman, C. D. Kurth, L. M. Montenegro, *et al.*, "Arterial and venous contributions to near-infrared cerebral oximetry," Anesthesiology **93**(4), 947 (2000).
34. T. R. Cheatle, L. A. Potter, M. Cope, *et al.*, "Near-infrared spectroscopy in peripheral vascular disease," Br. J. Surg. **78**(4), 405 (2005).
35. M. Ghijsen, G. R. Lentsch, S. Gioux, *et al.*, "Quantitative real-time optical imaging of the tissue metabolic rate of oxygen consumption," J. Biomed. Opt. **23**(03), 1–12 (2018).
36. C. M. Bopp, D. K. Townsend, and T. J. Barstow, "Characterizing near-infrared spectroscopy responses to forearm post-occlusive reactive hyperemia in healthy subjects," Eur. J. Appl. Physiol. **111**(11), 2753 (2011).
37. T. B. Willingham, W. M. Southern, and K. K. McCully, "Measuring reactive hyperemia in the lower limb using near-infrared spectroscopy," J. Biomed. Opt. **21**(9), 091302 (2016).
38. T. Quang, "Diffuse optical spectroscopy data of skeletal muscle and cerebral tissue of SCD patients," figshare, 2024, https://doi.org/10.6084/m9.figshare.26035687.
39. R. Rubinshtein, J. T. Kuvin, M. Soffler, *et al.*, "Assessment of endothelial function by non-invasive peripheral arterial tonometry predicts late cardiovascular adverse events," Eur. Heart J. **31**(9), 1142–1148 (2010).
40. Y. Matsuzawa, T.-G. Kwon, R. J. Lennon, *et al.*, "Prognostic value of flow-mediated vasodilation in brachial artery and fingertip artery for cardiovascular events: a systematic review and meta-analysis," J. Am. Heart Assoc. **4**(11), e002270 (2015).
41. J. Mesquida, A. Caballer, L. Cortese, *et al.*, "Peripheral microcirculatory alterations are associated with the severity of acute respiratory distress syndrome in COVID-19 patients admitted to intermediate respiratory and intensive care units," Crit. Care **25**(1), 381 (2021).
42. D. Milej, M. Shahid, A. Abdalmalak, *et al.*, "Characterizing dynamic cerebral vascular reactivity using a hybrid system combining time-resolved near-infrared and diffuse correlation spectroscopy," Biomed. Opt. Express **11**(8), 4571–4585 (2020).
43. J. Selb, D. A. Boas, S. T. Chan, *et al.*, "Sensitivity of near-infrared spectroscopy and diffuse correlation spectroscopy to brain hemodynamics: simulations and experimental findings during hypercapnia," Neurophotonics **1**(1), 015005 (2014).
44. K. P. Guilliams, M. E. Fields, D. K. Ragan, *et al.*, "Red cell exchange transfusions lower cerebral blood flow and oxygen extraction fraction in pediatric sickle cell anemia," Blood **131**(9), 1012–1021 (2018).
45. M. Nahavandi, J. P. Nichols, M. Hassan, *et al.*, "Near-infrared spectra absorbance of blood from sickle cell patients and normal individuals," Hematology **14**(1), 46–48 (2009).
46. A. Cerussi, R. Van Woerkom, F. Waffarn, *et al.*, "Noninvasive monitoring of red blood cell transfusion in very low birthweight infants using diffuse optical spectroscopy," J. Biomed. Opt. **10**(5), 051401 (2005).
47. S. Y. Lee, R. O. Brothers, K. B. Turrentine, *et al.*, "Quantifying the Cerebral Hemometabolic Response to Blood Transfusion in Pediatric Sickle Cell Disease With Diffuse Optical Spectroscopies," Front. Neurol. **13**, 869117 (2022).
48. E. Kucukal, Y. Man, E. Quinn, *et al.*, "Red blood cell adhesion to ICAM-1 is mediated by fibrinogen and is associated with right-to-left shunts in sickle cell disease," Blood Adv. **4**(15), 3688–3698 (2020).
49. C. Lawson and S. Wolf, "ICAM-1 signaling in endothelial cells," Pharmacol Rep. **61**(1), 22–32 (2009).
50. A. S. Hansen, J. H. Butt, S. Holm-Yildiz, *et al.*, "Validation of Repeated Endothelial Function Measurements Using EndoPAT in Stroke," Front. Neurol. **8**, 178 (2017).

Biomedical Optics EXPRESS

51. R. M. Bruno, T. Gori, and L. Ghiadoni, "Endothelial function testing and cardiovascular disease: focus on peripheral arterial tonometry," Vasc. Health Risk Manag. **10**, 577–584 (2014).
52. A. C. Philpott, E. Lonn, L. M. Title, *et al.*, "Comparison of New Measures of Vascular Function to Flow Mediated Dilatation as a Measure of Cardiovascular Risk Factors," Am. J. Cardiol. **103**(11), 1610–1615 (2009).
53. T. P. Whitton and W. J. Healy, "Clinical Use and Interpretation of Thromboelastography," ATS Sch. **4**(1), 96–97 (2023).
54. E. Sparkenbaugh and R. Pawlinski, "Interplay between coagulation and vascular inflammation in sickle cell disease," Br. J. Haematol. **162**(1), 3–14 (2013).
55. K. I. Ataga, C. G. Moore, C. A. Hillery, *et al.*, "Coagulation activation and inflammation in sickle cell disease-associated pulmonary hypertension," Haematologica **93**(1), 20 (2008).
56. M. Ghijsen, T. B. Rice, B. Yang, *et al.*, "Wearable speckle plethysmography (SPG) for characterizing microvascular flow and resistance," Biomed. Opt. Express **9**(8), 3937 (2018).
57. F. Scholkmann, S. Kleiser, A. J. Metz, *et al.*, "A review on continuous wave functional near-infrared spectroscopy and imaging instrumentation and methodology," NeuroImage **85**, 6–27 (2014).